

# Role of pressure in generation of intense velocity gradients in turbulent flows

Dhawal Buaria<sup>1,2,\*</sup> and Alain Pumir<sup>3,2</sup>

<sup>1</sup>*Tandon School of Engineering, New York University, New York, NY 11201, USA*

<sup>2</sup>*Max Planck Institute for Dynamics and Self-Organization, 37077 Göttingen, Germany*

<sup>3</sup>*Ecole Normale Supérieure, Université de Lyon 1 and CNRS, 69007 Lyon, France*

(Dated: August 9, 2023)

We investigate the role of pressure, via its Hessian tensor  $\mathbf{H}$ , on amplification of vorticity and strain-rate and contrast it with other inviscid nonlinear mechanisms. Results are obtained from direct numerical simulations of isotropic turbulence with Taylor-scale Reynolds number in the range 140 – 1300. Decomposing  $\mathbf{H}$  into local isotropic ( $\mathbf{H}^I$ ) and nonlocal deviatoric ( $\mathbf{H}^D$ ) components reveals that  $\mathbf{H}^I$  depletes vortex stretching (VS), whereas  $\mathbf{H}^D$  enables it, with the former slightly stronger. The resulting inhibition is significantly weaker than the nonlinear mechanism which always enables VS. However, in regions of intense vorticity, identified using conditional statistics, contribution from  $\mathbf{H}$  dominates over nonlinearity, leading to overall depletion of VS. We also observe near-perfect alignment between vorticity and the eigenvector of  $\mathbf{H}$  corresponding to the smallest eigenvalue, which conforms with well-known vortex-tubes. We discuss the connection between this depletion, essentially due to (local)  $\mathbf{H}^I$ , and recently identified self-attenuation mechanism [Buaria et al. *Nat. Commun.* 11:5852 (2020)], whereby intense vorticity is locally attenuated through inviscid effects. In contrast, the influence of  $\mathbf{H}$  on strain-amplification is weak. It opposes strain self-amplification, together with VS, but its effect is much weaker than VS. Correspondingly, the eigenvectors of strain and  $\mathbf{H}$  do not exhibit any strong alignments. For all results, the dependence on Reynolds number is very weak. In addition to the fundamental insights, our work provides useful data and validation benchmarks for future modeling endeavors, for instance in Lagrangian modeling of velocity gradient dynamics, where conditional  $\mathbf{H}$  is explicitly modeled.

## I. INTRODUCTION

A defining feature of turbulent flows is the generation of small scale structures, leading to dramatic enhancement of transport rates of mass, momentum and energy. In this regard, the importance of statistical properties of the velocity gradient tensor  $\mathbf{A} = \nabla \mathbf{u}$ , where  $\mathbf{u}$  is the velocity field, is well recognized [1–6]. By taking the derivative of the incompressible Navier-Stokes equations, the dynamics of  $\mathbf{A}$  are given by the following transport equation

$$\frac{DA_{ij}}{Dt} = -A_{ik}A_{kj} - H_{ij} + \nu \nabla^2 A_{ij} \quad (1)$$

where  $D/Dt$  is the material derivative,  $\nu$  is the kinematic viscosity,  $H_{ij} = \partial^2 P / \partial x_i \partial x_j$  is the pressure Hessian tensor; and the incompressibility condition imposes  $A_{ii} = 0$ . The quadratic non-linearity in Eq. (1) captures the self-amplification of velocity gradients, which leads to intermittent generation of extreme events and small scale structures in the flow. Owing to their practical significance in various physical processes [7–11], their postulated universality [1, 2, 12], as well as their connection to potential singularities of Euler and Navier-Stokes equations [13–15], the study of small scales and velocity gradients is of obvious importance in turbulence theory and modeling.

As implied by Eq. (1), the dynamics of velocity gradients are influenced by the pressure Hessian tensor. This leads to a nonlocal coupling of the entire gradient field, since pressure satisfies the Poisson equation:  $\nabla^2 P = -A_{ij}A_{ji}$ , as obtained by taking the trace of Eq. (1). The mathematical difficulties posed by this nonlocality makes it very hard to decipher the precise role of pressure Hessian on gradient amplification and the formation of extreme events. In general, it has been observed that pressure Hessian acts to counteract the nonlinear amplification [5, 16–20]. Since the pressure Hessian is a symmetric tensor, its influence on the amplification of strain, the symmetric part of the  $\mathbf{A}$ , is more explicit [16, 21]. In contrast, its influence on vorticity, the skew-symmetric part of  $\mathbf{A}$ , is indirectly felt through strain, and much more difficult to understand. The interaction between vorticity and strain itself is an indispensable ingredient of turbulence. For instance, it is well established that vorticity preferentially aligns with the eigenvector corresponding to the intermediate eigenvalue of the strain tensor, which in turn is positive on average [5, 22]. Additionally, this alignment is considerably stronger in regions of intense vorticity and strain [20, 23]. In contrast, the role of pressure Hessian, especially in regions of intense vorticity or strain has received little or no attention.

---

\* dhawal.buaria@nyu.edu

Prior studies predominantly focused on unconditional statistics, which do not distinguish quiescent regions from regions where extreme events reside. Additionally, they have also been restricted to low Reynolds numbers [16, 18, 24]. It is well known that extreme vorticity and strain events in turbulence have a pronounced structure, where the statistical properties can be very different than the mean field [5, 20, 23, 25, 26]. Thus, analyzing statistics conditioned on the magnitude of vorticity or strain can be particularly useful to understand the underlying amplification mechanism [5, 20, 23]. In addition to providing fundamental insights, conditional statistics of pressure Hessian also play a central role in turbulence modeling, particularly Lagrangian modeling of velocity gradient dynamics [6, 18, 27–30].

In this work, our objective is to systematically analyze the effect of pressure Hessian on amplification of vorticity and strain. We identify and analyze various correlations between the pressure Hessian and vorticity and strain fields. We consider unconditional statistics and also statistics conditioned on magnitude of vorticity and strain, to focus on extreme events. It is worth noting that strain itself can be nonlocally related to vorticity, via the Biot-Savart integral, providing an alternative way to study the nonlocality of gradient amplification—without invoking pressure—by filtering strain into scale-wise contributions [21, 31, 32]. Alternatively, the pressure Hessian tensor itself can also be filtered into scale-wise contributions [33]. Complementary to these approaches, our focus here is to directly analyze the pressure Hessian term to directly investigate its role on gradient amplification.

To that end, the necessary statistics are extracted from state-of-the-art direct numerical simulations of isotropic turbulence in periodic domains, which is the most efficient numerical tool to study the small-scale properties of turbulence. One important purpose of the current study is also to understand the effect of increasing Reynolds number. To this end, we utilize a massive DNS database with Taylor-scale Reynolds number  $R_\lambda$  ranging from 140 to 1300, on up to grid sizes of  $12288^3$ ; particular attention is given on having good small-scale resolution to accurately resolve the extreme events [20, 23, 34], for which conditional statistics are analyzed.

The manuscript is organized as follows. The necessary background for our analysis is briefly reviewed in § 2. The numerical approach and DNS database is presented in § 3. In § 4, the role of pressure Hessian is analyzed in the context of vorticity amplification, whereas in § 5 the analysis is in the context of strain amplification. Finally, we summarize our results in § 5.

## II. BACKGROUND

The vorticity vector  $\boldsymbol{\omega}$  and the strain tensor  $\mathbf{S}$ , defined as:  $\omega_i = \varepsilon_{ijk}A_{jk}$  ( $\varepsilon_{ijk}$  being the Levi-Civita symbol) and  $S_{ij} = (A_{ij} + A_{ji})/2$ , respectively represent the skew-symmetric and symmetric components of the velocity gradient tensor, and characterize the local rotational and stretching motions. Their evolution equations can be readily obtained from Eq. (1) and are given as

$$\frac{D\omega_i}{Dt} = \omega_j S_{ij} + \nu \nabla^2 \omega_i, \quad (2)$$

$$\frac{DS_{ij}}{Dt} = -S_{ik}S_{kj} - \frac{1}{4}(\omega_i\omega_j - \omega^2\delta_{ij}) - H_{ij} + \nu \nabla^2 S_{ij}. \quad (3)$$

The non-linear amplification of vorticity is captured by the vortex stretching vector  $W_i = \omega_j S_{ij}$ , whereas amplification of strain is controlled by the self-amplification term and additionally via feedback of vorticity. Although the pressure Hessian, which is a symmetric tensor, only contributes to evolution of strain, it still indirectly affects vorticity, since the pressure Poisson couples both vorticity and strain. Indeed, taking the trace of Eq. (3), gives  $\nabla^2 P = (\omega_i\omega_i - 2S_{ij}S_{ij})/2$ . The influence of pressure Hessian on vorticity becomes apparent when considering the evolution equation for the vortex stretching vector

$$\frac{DW_i}{Dt} = -\omega_j H_{ij} + \text{viscous terms}, \quad (4)$$

Note that  $DW_i/Dt = D^2\omega_i/Dt^2$  in the inviscid limit, which directly relates the pressure Hessian to the second derivative of vorticity.

To quantify the intensity of gradients, we consider the magnitudes of vorticity and strain [34, 35]

$$\Omega = \omega_i\omega_i, \quad \Sigma = 2S_{ij}S_{ij}, \quad (5)$$

where the former is the enstrophy, and the latter is dissipation rate  $\epsilon$  divided by viscosity, i.e.,  $\Sigma = \epsilon/\nu$ . In homogeneous turbulence,  $\langle \Omega \rangle = \langle \Sigma \rangle = 1/\tau_K^2$ , where  $\tau_K$  is the Kolmogorov time scale. Likewise, it is useful to consider transport

equations for these quantities

$$\frac{1}{2} \frac{D\Omega}{Dt} = \omega_i \omega_j S_{ij} + \nu \omega_i \nabla^2 \omega_i, \quad (6)$$

$$\frac{1}{4} \frac{D\Sigma}{Dt} = -S_{ij} S_{jk} S_{ki} - \frac{1}{4} \omega_i \omega_j S_{ij} - S_{ij} H_{ij} + \nu S_{ij} \nabla^2 S_{ij} \quad (7)$$

The amplification of enstrophy is engendered by the term  $\omega_i \omega_j S_{ij} = \omega_i W_i$ , which in turn evolves according to:

$$\frac{D\omega_i W_i}{Dt} = W_i W_i - \omega_i \omega_j H_{ij} + \text{viscous terms}. \quad (8)$$

In the inviscid limit,  $D(\omega_i W_i)/Dt = D^2\Omega/Dt^2$ , thus Eq. (8) is complementary to Eq. (4) for  $W_i$ . The above equations identify the correlations responsible for generation of intense velocity gradients, which we will analyze, both unconditionally and conditioned on magnitudes of  $\Omega$  and  $\Sigma$ .

For our analysis, it is also useful to consider the eigenframes of the strain and pressure Hessian tensors. For the strain tensor, it is defined by the eigenvalues  $\lambda_i$  (for  $i = 1, 2, 3$ ), such that  $\lambda_1 \geq \lambda_2 \geq \lambda_3$  and the corresponding eigenvectors  $\mathbf{e}_i$ . Incompressibility gives  $\lambda_1 + \lambda_2 + \lambda_3 = 0$ , implying that  $\lambda_1$  is always positive (stretching) and  $\lambda_3$  is always negative (compressive). Similarly, the eigenframe of pressure Hessian is given by the eigenvalues  $\lambda_i^P$  (in descending order), and eigenvectors  $\mathbf{e}_i^P$ . In this case, incompressibility gives  $H_{ii} = \nabla^2 P = \lambda_1^P + \lambda_2^P + \lambda_3^P$ , which is in general non-zero. Thus, it is convenient to decompose the pressure Hessian into isotropic and deviatoric components:

$$H_{ij}^I = \frac{H_{kk}}{3} \delta_{ij}, \quad \text{with } H_{kk} = \nabla^2 P = (\Omega - \Sigma)/2, \quad (9)$$

$$H_{ij}^D = H_{ij} - H_{ij}^I. \quad (10)$$

Note, since  $\mathbf{H}^I$  can be explicitly expressed in terms of  $\mathbf{A}$ , it can be considered local, whereas  $\mathbf{H}^D$  captures the nonlocality of the pressure field [36]. The eigenvalues  $\lambda_i^D$  of  $H_{ij}^D$  satisfy  $\lambda_i^D = \lambda_i^P - H_{kk}/3$  and hence,  $\lambda_1^D + \lambda_2^D + \lambda_3^D = 0$ , implying  $\lambda_1^D > 0$  and  $\lambda_3^D < 0$ ; whereas the eigenvectors are unaffected, i.e.,  $\mathbf{e}_i^D = \mathbf{e}_i^P$ . Using this framework, we obtain

$$\omega_i \omega_j H_{ij} = \lambda_i^P (\mathbf{e}_i^P \cdot \boldsymbol{\omega})^2, \quad \omega_i \omega_j H_{ij}^D = \lambda_i^D (\mathbf{e}_i^P \cdot \boldsymbol{\omega})^2, \quad \omega_i \omega_j H_{ij}^I = \Omega(\Omega - \Sigma)/6, \quad (11)$$

which decomposes the correlation between vorticity and pressure Hessian into individual contribution from each eigendirection. Similarly, the terms  $\omega_i W_i$  and  $W_i W_i$  can be decomposed in the eigenframe of the strain tensor, illustrating the importance of the alignments between vorticity vector and the eigenvectors of strain. We refer to our recent works [20, 23] for a discussion of these properties. On the other hand, the contribution  $S_{ij} H_{ij}$  in Eq. (7) can be written as

$$S_{ij} H_{ij} = \lambda_i^P \lambda_j (\mathbf{e}_i^P \cdot \mathbf{e}_j)^2. \quad (12)$$

Since,  $S_{ij} H_{ij}^I = 0$  from incompressibility, it also follows that

$$S_{ij} H_{ij} = S_{ij} H_{ij}^D = \lambda_i^D \lambda_j (\mathbf{e}_i^P \cdot \mathbf{e}_j)^2. \quad (13)$$

### III. NUMERICAL APPROACH AND DATABASE

The data utilized here are the same as in several recent works [21, 23, 32, 37–39] and are generated using direct numerical simulations (DNS) of incompressible Navier-Stokes equations, for the canonical setup of isotropic turbulence in a periodic domain. The simulations are carried out using highly accurate Fourier pseudo-spectral methods with second-order Runge-Kutta integration in time, and the large scales are forced numerically to achieve statistical stationarity [40]. A key characteristic of our data is that we have achieved a wide range of Taylor-scale Reynolds number  $R_\lambda$ , going from 140 – 1300, while maintaining excellent small-scale resolution, which is as high as  $k_{\max} \eta \approx 6$ , where  $k_{\max} = \sqrt{2}N/3$ , is the maximum resolved wavenumber on a  $N^3$  grid, and  $\eta$  is the Kolmogorov length scale. Convergence with respect to resolution and statistical sampling has been adequately established in previous works. For convenience, we summarize the DNS database and the simulation parameters in Table I; additional details can be obtained in our prior works cited earlier.

$R_\lambda$	$N^3$	$k_{max}\eta$	$T_E/\tau_K$	$T_{sim}$	$N_s$
140	1024 <sup>3</sup>	5.82	16.0	6.5 $T_E$	24
240	2048 <sup>3</sup>	5.70	30.3	6.0 $T_E$	24
390	4096 <sup>3</sup>	5.81	48.4	2.8 $T_E$	35
650	8192 <sup>3</sup>	5.65	74.4	2.0 $T_E$	40
1300	12288 <sup>3</sup>	2.95	147.4	20 $\tau_K$	18

TABLE I. Simulation parameters for the DNS runs used in the current work: the Taylor-scale Reynolds number ( $R_\lambda$ ), the number of grid points ( $N^3$ ), spatial resolution ( $k_{max}\eta$ ), ratio of large-eddy turnover time ( $T_E$ ) to Kolmogorov time scale ( $\tau_K$ ), length of simulation ( $T_{sim}$ ) in statistically stationary state and the number of instantaneous snapshots ( $N_s$ ) used for each run to obtain the statistics.

$R_\lambda$	$\langle\lambda_i^P\rangle$	$\langle(\mathbf{e}_i^P \cdot \hat{\boldsymbol{\omega}})^2\rangle$	$\langle\omega_i\omega_j H_{ij}^D\rangle$	$\langle\omega_i\omega_j H_{ij}^I\rangle$	$\langle\omega_i\omega_j H_{ij}\rangle$	$\langle W_i W_i\rangle$
140	0.295 : 0.024 : -0.319	0.290 : 0.416 : 0.294	-0.363	0.410	0.047	0.146
240	0.301 : 0.025 : -0.326	0.292 : 0.418 : 0.290	-0.483	0.549	0.066	0.180
390	0.302 : 0.025 : -0.327	0.292 : 0.418 : 0.290	-0.587	0.670	0.083	0.216
650	0.304 : 0.026 : -0.330	0.293 : 0.418 : 0.289	-0.746	0.853	0.107	0.269
1300	0.305 : 0.026 : -0.331	0.293 : 0.418 : 0.289	-1.010	1.153	0.146	0.360

TABLE II. Unconditional averages of various quantities associated with correlation of vorticity and pressure Hessian, based on Eq. (8).  $\lambda_i^P$ , for  $i = 1, 2, 3$ , are the eigenvalues of pressure Hessian, with corresponding eigenvectors  $\mathbf{e}_i^P$ . All quantities are appropriately normalized by the Kolmogorov time scale  $\tau_K$ .

## IV. ROLE OF PRESSURE HESSIAN ON VORTICITY AMPLIFICATION

### A. Unconditional statistics

Table II lists various unconditional statistics characterizing the role of pressure Hessian on vortex stretching, based on Eq. (8), at different  $R_\lambda$ . All quantities are appropriately non-dimensionalized by the Kolmogorov time scale  $\tau_K$ , and henceforth, should be interpreted as such (unless otherwise mentioned). We first consider the eigenvalues of pressure Hessian. Owing to homogeneity  $\langle H_{ii} \rangle = 0$ ; thus,  $\sum_{i=1}^3 \langle \lambda_i^P \rangle = 0$  and  $\langle \lambda_i^P \rangle = \langle \lambda_i^D \rangle$ . Table II reveals that the individual averages of the eigenvalues are approximately equal to  $0.3 : 0.03 : -0.33$ , without any appreciable dependence on  $R_\lambda$ . The intermediate eigenvalue is overall positive on average but its magnitude is substantially smaller than the other two, and essentially close to zero.

Similarly, the mean square of alignment cosines between vorticity and eigenvectors of pressure Hessian,  $\langle (\mathbf{e}_i^P \cdot \hat{\boldsymbol{\omega}})^2 \rangle$ , where  $\hat{\boldsymbol{\omega}}$  denotes the unit vector parallel to  $\boldsymbol{\omega}$ , are also essentially independent of  $R_\lambda$ . Note that the square of cosines sum up to unity for all three directions. Additionally, they are bounded between 0 and 1 for each individual direction, respectively for the case of perfect orthogonal and parallel alignment; whereas for a uniform distribution of the alignment cosine, the mean square average is  $1/3$ . From Table II, we observe that the measured alignments do not deviate significantly from  $1/3$ , with a weak preferential alignment of vorticity with the intermediate eigenvector of the pressure Hessian.

It is worth noting that while a uniform distribution of the alignment cosine implies the second moment is  $1/3$ , the reverse is not necessarily true. Thus, it is useful to also inspect the probability density function (p.d.f.) of the alignment cosines, which are shown in Fig. 2. The solid and dashed curves respectively correspond to  $R_\lambda = 1300$  and  $140$ , demonstrating that the alignments are independent of  $R_\lambda$ . The distributions for  $|\mathbf{e}_1^P \cdot \hat{\boldsymbol{\omega}}|$  and  $|\mathbf{e}_3^P \cdot \hat{\boldsymbol{\omega}}|$  conform with expectation from their second moments in Table II, respectively indicating weak preferential orthogonal and parallel alignment. However, for  $|\mathbf{e}_2^P \cdot \hat{\boldsymbol{\omega}}|$ , we observe an anomalous behavior, showing simultaneous preferential orthogonal and parallel alignments, which cancel each other out when evaluating the second moment. Note that the limiting cases of 0 or 1 for the second moment of alignment cosines do not present such an anomaly for the PDFs. In fact, we will see later that when considering conditional statistics, the alignments are substantially enhanced for extreme vorticity events (such that using the second moment only does not lead to any ambiguity).

Finally, we consider the net contributions to the budget of vortex stretching (as per Eq. (8)). Table II shows separately the mean contributions from the deviatoric and isotropic components of the pressure Hessian and their sum  $\langle \omega_i \omega_j H_{ij} \rangle$ , contrasted with the nonlinear term  $\langle W_i W_i \rangle$ . Remarkably, the deviatoric and isotropic contributions, are comparable in magnitude but opposite in sign. Taking into account the negative sign before the pressure Hessian term in Eq.(8), it follows that  $\mathbf{H}^D$  favors vortex stretching, whereas  $\mathbf{H}^I$  inhibits it. This essentially establishes that nonlocal effects of the pressure field enable vortex stretching [36], conforming with earlier studies that vortex stretching

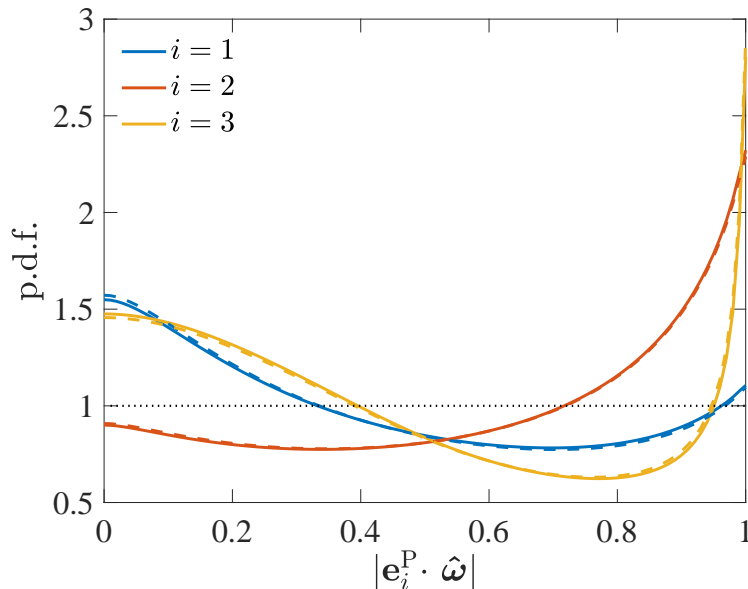


FIG. 1. Probability density function (p.d.f.) of alignment cosines between vorticity and eigenvectors of pressure Hessian, at  $R_\lambda = 1300$  (solid lines) and  $R_\lambda = 140$  (dashed lines).

is predominantly nonlocal [21, 31, 32]. We will further elaborate on this effect later.

The strong cancellation between the deviatoric and isotropic contributions results in a weakly positive value of  $\langle \omega_i \omega_j H_{ij} \rangle$ , implying that pressure Hessian overall weakly opposes vortex stretching – which is primarily a local effect stemming from the dominant isotropic contribution of pressure Hessian. Both the deviatoric and isotropic contributions become stronger with  $R_\lambda$ , but the latter is always slightly dominant. In contrast, the term  $W_i W_i$ , listed last in Table II, is positive by definition, and thus always enables vortex stretching. This term increases with  $R_\lambda$  and is noticeably larger than  $\langle \omega_i \omega_j H_{ij} \rangle$  (at all  $R_\lambda$ ). This leads to the (anticipated) result that the nonlinear effects in turbulence predominantly enable vortex stretching, with a net positive energy cascade from large to small scales [41–43]. Although not shown, the  $R_\lambda$  dependence of these quantities conforms with an approximate power law of  $R_\lambda^{0.39}$  in nominal agreement with fourth order moment of velocity derivatives [44, 45].

## B. Conditional statistics

In the previous subsection, we considered unconditional statistics, which provide an overall perspective of the flow. To specifically characterize the extreme events or regions of intense vorticity, we condition the statistics on the magnitude of vorticity; specifically, we will use  $\Omega \tau_K^2$ , (or equivalently,  $\Omega / \langle \Omega \rangle$ ), to quantify the extremeness of an event with respect to the mean field.

Figure 2 shows the conditional mean square of alignment cosines between vorticity and the eigenvectors of pressure Hessian, at various  $R_\lambda$ . For weak enstrophy, all the curves are at  $1/3$ , consistent with a uniform distribution of cosines. For  $\Omega \tau_K^2 \approx 1$ , we notice that vorticity has a weak preferential alignment with  $\mathbf{e}_2^P$ , in agreement with the unconditional results in Table II. However, for extreme events, a different picture emerges and vorticity almost perfectly aligns with  $\mathbf{e}_3^P$  (becoming orthogonal to both first and second eigenvectors). This alignment can be explained by considering the familiar picture of intense vorticity being arranged in tube-like structures [25, 34, 46], as discussed at the end of the present subsection.

Figure 3 shows the conditional expectation of the eigenvalues of pressure Hessian. To focus on extreme events, the abscissa is set to  $\Omega \tau_K^2 \geq 1$ . The identity  $\sum_i \lambda_i^P = \nabla^2 P = (\Omega - \Sigma)/2$  implies that  $\sum_i \langle \lambda_i^P | \Omega \rangle = (\Omega - \langle \Sigma | \Omega \rangle)/2$ . Recent numerical works [23, 34, 35] have shown that for large enstrophy,  $\langle \Sigma | \Omega \rangle \sim \Omega^\gamma$ , where the exponent  $\gamma < 1$ , but weakly increases with  $R_\lambda$  (with  $\gamma \rightarrow 1$  being the asymptotic limit). Thus, while the average sum of eigenvalues is zero for the mean field, it is strongly positive in regions of intense enstrophy. In fact, to the leading order, one can anticipate that  $\langle \lambda_i^P | \Omega \rangle \sim \Omega$  when  $\Omega \tau_K^2 \gg 1$ . Figure 3a shows the quantity  $\langle \lambda_i^P | \Omega \rangle / \Omega$ . The behavior of the averaged eigenvalues at  $\Omega \tau_K^2 = 1$  is consistent with the results in Table II. However, in regions of intense enstrophy, the first two eigenvalues are strongly positive, whereas the third eigenvalue is essentially zero. Once again, no appreciable dependence on  $R_\lambda$  is seen for this case.

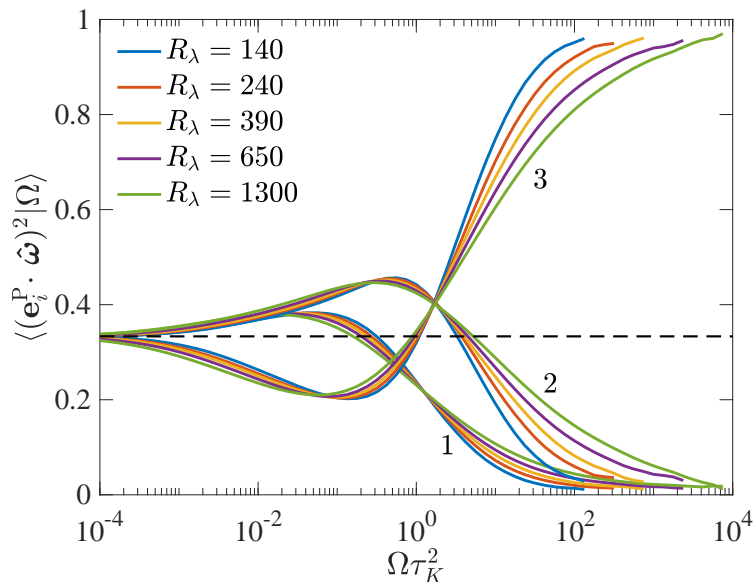


FIG. 2. Conditional expectation (given enstrophy  $\Omega$ ) of second moment of alignment cosines between vorticity unit vector ( $\hat{\boldsymbol{\omega}}$ ) and eigenvectors of pressure Hessian ( $\mathbf{e}_i^P$ ), at various  $R_\lambda$ .

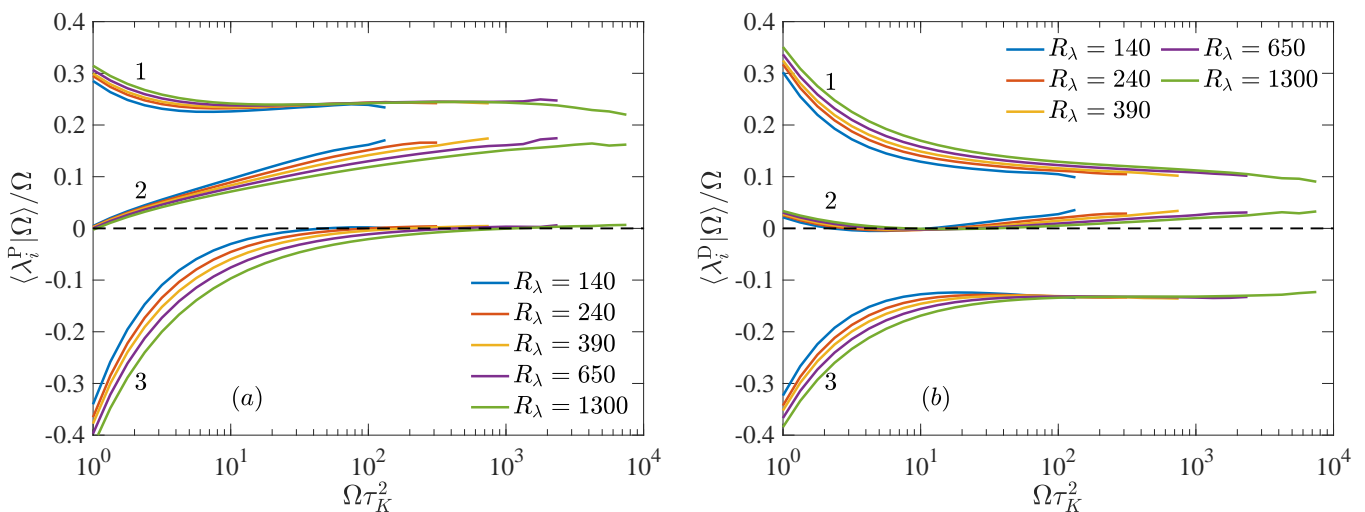


FIG. 3. (a) Conditional expectations (given enstrophy  $\Omega$ ) of the eigenvalues of pressure Hessian, for various  $R_\lambda$ . (b) Conditional expectations of the eigenvalues of the deviatoric part. The legend in panel (b) also applies to (a).

Given that vorticity is almost perfectly aligned with third eigenvector of pressure Hessian and the corresponding eigenvalue is close to zero, the behavior of the term  $\omega_i \omega_j H_{ij}$  cannot be easily inferred. Figure 4a shows the conditional expectation  $\langle \omega_i \omega_j H_{ij} | \Omega \rangle / \Omega^2$ , along with the individual contributions in each eigendirection. The normalization by  $\Omega^2$  comes from simple dimensional grounds. For  $\Omega \tau_K^2 \simeq 1$ , the contributions from first and third eigendirections are expectedly positive and negative, respectively, largely canceling each other to give a weakly positive net contribution (whereas the contribution from second direction is essentially negligible). However, for  $\Omega \tau_K^2 \gg 1$ , the contributions from all directions become positive and comparable. Thus, in regions of intense vorticity, the role of pressure (Hessian) is to oppose vortex stretching.

To better understand this result, we consider next the contributions from the deviatoric and the isotropic components of the pressure Hessian. The sum of eigenvalues of the deviatoric part  $\mathbf{H}^D$  is always constrained to be zero, i.e.,  $\sum_i \lambda_i^D = 0$ , and thus,  $\sum_i \langle \lambda_i^D | \Omega \rangle = 0$ . Figure 3b shows the conditional expectation  $\langle \lambda_i^D | \Omega \rangle / \Omega$ . While the results shown in Fig. 3b for  $\Omega \tau_K^2 \simeq 1$  are essentially identical to  $\langle \lambda_i^P | \Omega \rangle$ , the behavior for  $\Omega \tau_K^2 \gg 1$  is different, with the first and second eigenvalues being always positive (with the second being noticeably weaker), whereas third eigenvalue is always negative (perfectly canceling the contribution from other two). Thus, from the results in Figs. 2 and 3b, it

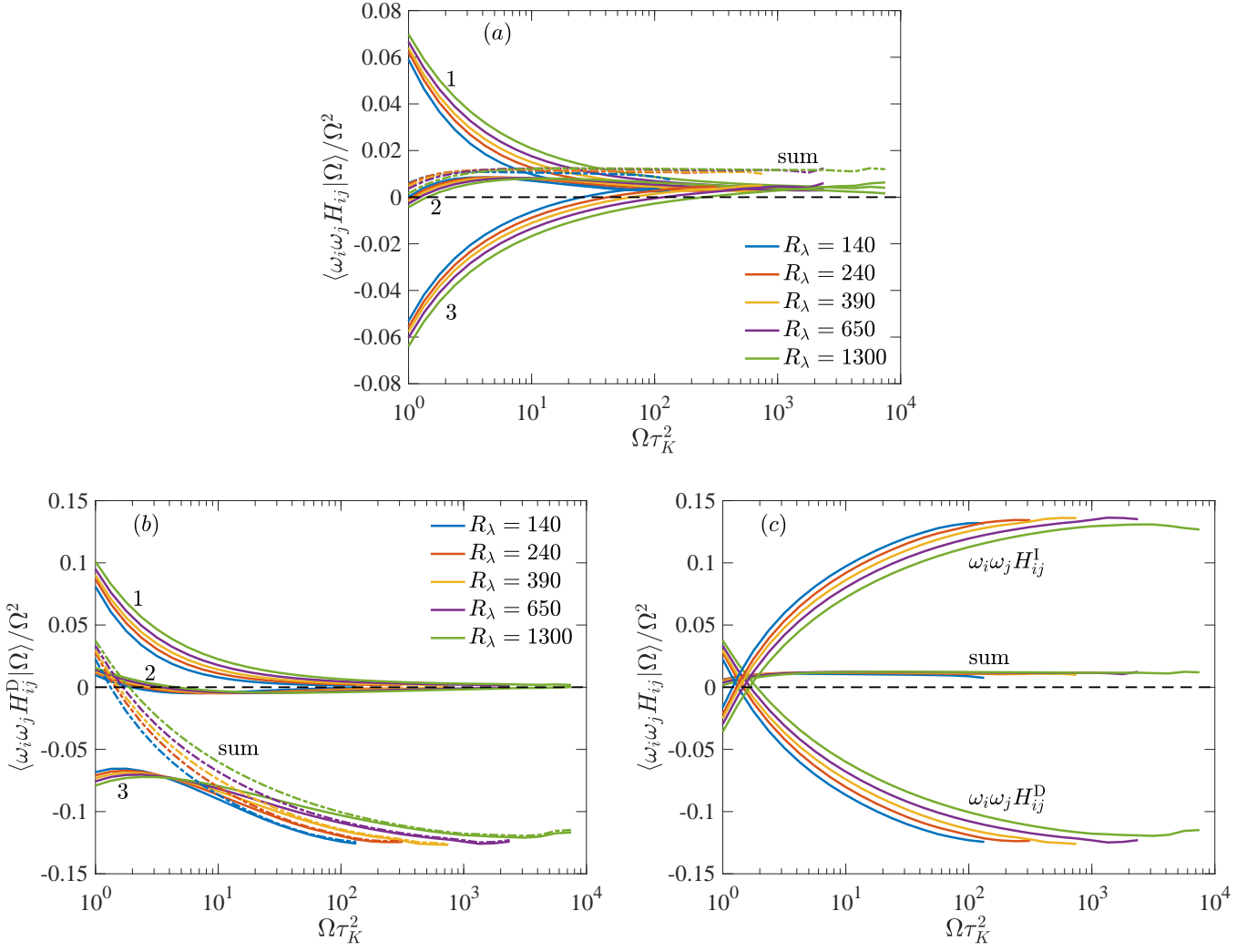


FIG. 4. (a) Conditional expectation (given enstrophy  $\Omega$ ) of the term  $\omega_i \omega_j H_{ij}$  (marked as sum) and individual contributions from each eigendirection of pressure Hessian (in solid lines). The quantities are normalized by  $\Omega^2$  to reveal a plateau like behavior for  $\Omega\tau_K^2 \gg 1$ . (b) Same as a, but for  $\omega_i \omega_j H_{ij}^D$ , (the contribution from the deviatoric part of pressure Hessian). (c) The net contributions from a and b are further contrasted with  $\omega_i \omega_j H_{ij}^I$  (the contribution from isotropic part of pressure Hessian).

can be anticipated that  $\langle \omega_i \omega_j H_{ij}^D | \Omega \rangle$  is negative in regions of intense enstrophy. The contribution of the isotropic component is also easy to understand, since  $\langle \omega_i \omega_j H_{ij}^I | \Omega \rangle = \langle \Omega(\Omega - \Sigma) | \Omega \rangle / 6 = (\Omega^2 - \Omega \langle \Sigma | \Omega \rangle) / 6$ . Using  $\langle \Sigma | \Omega \rangle \sim \Omega^\gamma$  (with  $\gamma < 1$ ) implies that  $\langle \omega_i \omega_j H_{ij}^I | \Omega \rangle$  is positive in regions of intense enstrophy. We verify these expectations in Fig. 4b-c.

Figure 4b shows the conditional expectation  $\langle \omega_i \omega_j H_{ij}^D | \Omega \rangle / \Omega^2$ , along with the individual contributions in each eigendirection. It can be clearly seen that for large enstrophy, the contributions from both first and second eigendirections are essentially zero and the third eigendirection completely dominates the overall sum (as explained earlier). This again establishes that the nonlocal portion of the pressure Hessian actually enables vortex stretching. In Fig. 4c, we compare the contributions from the deviatoric and isotropic components, together with the overall average. We notice that the isotropic contribution is strongly positive, canceling the deviatoric contribution to give a weakly net positive average. Once again, this shows that the depletion of vortex stretching by pressure Hessian is local.

It is worth noting that many qualitative aspects of the previously discussed results can be explained by noting that intense enstrophy is found in tube-like vortices [25, 34, 46], for which the Burgers vortex model is a good first order approximation [25, 47]. For the simple case of a Burgers vortex, pressure is minimum and constant along the axis of the vortex. This implies that the smallest (third) eigenvalue of pressure Hessian is zero and the corresponding eigenvector is perfectly aligned with vorticity; whereas the first two eigenvalues are positive and the corresponding eigenvectors are perfectly orthogonal to vorticity [48]. Indeed, these expectations are qualitatively consistent with

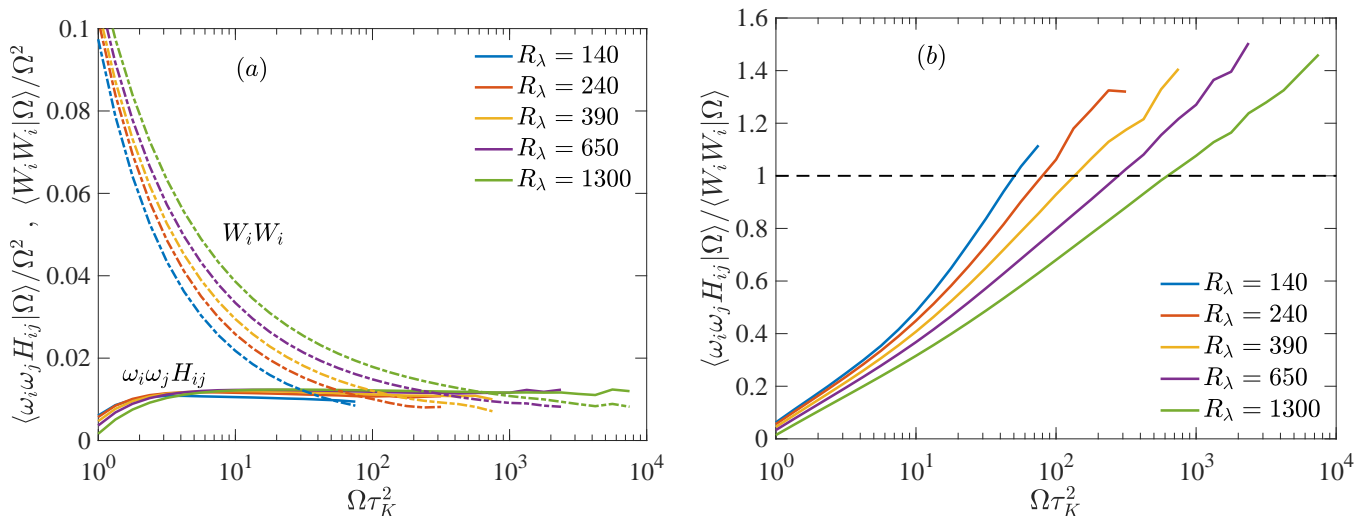


FIG. 5. (a) Conditional expectations (given enstrophy  $\Omega$ ) of the nonlinear and pressure Hessian contributions to the dynamics of vortex stretching vector, as given in Eq. (8). (a) The ratio of two terms, revealing that pressure Hessian contribution overtakes the nonlinear contribution at large  $\Omega$ .

the results shown in Figs. 2-3. However, we note that the precise structure of vortices in turbulence is different than Burgers vortex in some very crucial aspects. For instance, due to the structural properties of Burgers vortex, the term  $\omega_i \omega_j H_{ij}$  is essentially zero, which is not the case in turbulence. Additionally, vorticity is perfectly axial in Burgers vortex, but not real turbulent vortices, and there is some noticeable degree of Beltramization [21, 49] – an effect that is essential to the self-attenuation mechanism analyzed in [21, 32]. In fact, we will discuss in the next subsection that the net positive contribution from the pressure Hessian as observed in Fig. 4 is in fact connected to the self-attenuation mechanism observed in [21, 32].

### C. Contrasting nonlinear and pressure Hessian contributions

Table II demonstrates that the (unconditional) contribution  $\langle W_i W_i \rangle$  is substantially larger than  $\langle \omega_i \omega_j H_{ij} \rangle$  at all  $R_\lambda$ . A comparison of the conditional result is first made in Fig. 5a. Evidently, the nonlinear term dominates the pressure Hessian term at  $\Omega \tau_K^2 \simeq 1$ , in essential agreement with the observation in Table II. However, for intense enstrophy, we notice a substantial reduction in the nonlinear term  $\langle W_i W_i | \Omega \rangle / \Omega^2$  relative to the pressure Hessian term  $\langle \omega_i \omega_j H_{ij} | \Omega \rangle / \Omega^2$ , with the latter being approximately constant. Since  $W_i = \omega_j S_{ij}$ , it follows that  $\langle W_i W_i | \Omega \rangle \sim \langle \Omega \Sigma | \Omega \rangle \sim \Omega^{1+\gamma}$ . In contrast, we find  $\langle \omega_i \omega_j H_{ij} | \Omega \rangle \sim \Omega^2$ . Thus, the observation in Fig. 5a essentially shows that the pressure Hessian term grows significantly faster than the nonlinear term as  $\Omega$  increases, such that for large enough  $\Omega$ , the pressure Hessian contribution eventually becomes stronger than the nonlinear contribution (as indeed seen in Fig. 5a). To show this more clearly, Fig. 5b shows the ratio between the two terms, which is close to zero at  $\Omega \tau_K^2 = 1$ , but steadily increases and becomes greater than unity at large  $\Omega$  for every  $R_\lambda$ . Hence, the attenuating effect of pressure Hessian eventually prevails over the nonlinear term  $W_i W_i$ . Interestingly, the crossover point in  $\Omega$  increases with  $R_\lambda$ , which essentially is a reflection of intermittency and  $\gamma$  slowly increasing with  $R_\lambda$ .

Further insight on the attenuation induced by the pressure Hessian in regions of intense vorticity can be obtained by rewriting Eq. (8) for the conditional field

$$\frac{D \langle \omega_i W_i | \Omega \rangle}{Dt} = \langle W_i W_i | \Omega \rangle + (-\langle \omega_i \omega_j H_{ij}^D | \Omega \rangle) - (\langle \omega_i \omega_j H_{ij}^I | \Omega \rangle) + \text{viscous terms} \quad (14)$$

Note that the l.h.s. is not zero even in stationary turbulence. We essentially observe that the first two terms on the r.h.s. are positive, whereas the third term is negative, i.e., vortex stretching is enabled by the nonlinear term (which is local) and the deviatoric pressure Hessian (which is nonlocal), whereas the isotropic pressure Hessian (which is local) strongly opposes it. For weak or moderate  $\Omega$ , the positive contribution prevails, resulting in net positive rate of change of vortex stretching leading to increased vorticity amplification. However, for large  $\Omega$ , the negative contribution from  $H_{ij}^I$  prevails, leading to negative rate of change of vortex stretching. In all cases, the viscous terms are ignored, which are negligibly small at large  $R_\lambda$  (although not shown, this can be anticipated).



$R_\lambda$	$\langle(\mathbf{e}_1^P \cdot \mathbf{e}_j)^2\rangle$	$\langle(\mathbf{e}_2^P \cdot \mathbf{e}_j)^2\rangle$	$\langle(\mathbf{e}_3^P \cdot \mathbf{e}_j)^2\rangle$
140	0.231 : 0.401 : 0.368	0.377 : 0.373: 0.250	0.392 : 0.226 : 0.382
240	0.231 : 0.400 : 0.369	0.376 : 0.376: 0.249	0.393 : 0.224 : 0.383
390	0.231 : 0.400 : 0.369	0.376 : 0.376: 0.249	0.393 : 0.224 : 0.383
650	0.231 : 0.400 : 0.369	0.375 : 0.377: 0.248	0.394 : 0.223 : 0.383
1300	0.231 : 0.400 : 0.369	0.375 : 0.377: 0.248	0.394 : 0.223 : 0.383

TABLE III. Second moment of alignment cosines between the eigenvectors of pressure Hessian ( $\mathbf{e}_i^P$ ) and strain ( $\mathbf{e}_j$ ), at various  $R_\lambda$ .

We stress that, although the pressure Hessian is known to attenuate vortex stretching [24], the results in Fig. 5 indicate that this attenuation overwhelms even the nonlinear terms in regions of most intense vorticity. This points to an inviscid regularizing mechanism, which can be traced back to the prevalence of the contribution of  $H^I$ , which can be understood as local [36]. A very similar observation for attenuation of vorticity amplification was also recently uncovered in [21, 32]. In these works, the nonlocality of vortex stretching was analyzed by writing strain as the Biot-Savart integral of vorticity and decomposing it into local and nonlocal contributions. The local contribution is obtained by integrating in a sphere of radius  $R$ , whereas the remaining integral is the nonlocal contribution. Thereafter, it was observed that vortex stretching is engendered by the nonlocal contribution and remarkably, the local contribution acts to attenuate intense vorticity, also representing an inviscid mechanism to counter vorticity amplification. It stands to reason that the self-attenuation mechanism identified in [21, 32] is essentially related to the local pressure mechanism identified in this work. An important underlying connection between them is that they both act only when enstrophy becomes sufficiently strong and this critical value increases with  $R_\lambda$  [21]. Nevertheless, we note that precisely underpinning the causality between the two mechanisms requires further analysis, particularly by considering Lagrangian particle trajectories, as evident from Eq. (14). Such an analysis will be considered in a future work.

## V. ROLE OF PRESSURE HESSIAN ON STRAIN AMPLIFICATION

While the previous section focused on the role of the pressure Hessian on vorticity amplification, we characterize here the role of pressure Hessian on strain amplification, based on Eq. (7). Homogeneity implies that  $\langle S_{ij} H_{ij} \rangle = 0$ , so there is no net contribution from pressure Hessian to the budget of  $\Sigma$ . Nevertheless, the situation is quite different when isolating extreme events, with prior studies showing that pressure Hessian opposes strain amplification in regions of intense strain [16, 18, 20, 24] (and thus, amplifies weak strain). In our recent work [20], we already analyzed many aspects of strain amplification especially by focusing on individual eigenvalues of strain. Here, we present a complementary analysis focusing on eigenvalues of pressure Hessian, in the spirit of the analysis in the previous section.

### A. Unconditional statistics

We first analyze the alignments cosines between eigenvectors of strain and pressure Hessian, as measured by  $\langle(\mathbf{e}_i^P \cdot \mathbf{e}_j)^2\rangle$  for  $i, j = 1, 2, 3$ . The (unconditional) average of eigenvalues of the pressure Hessian can be found in Table II, whereas those of strain tensor were previously discussed in [23]. Table III lists all the nine individual terms for various  $R_\lambda$ , revealing no particularly strong alignment between the eigenvectors of strain and pressure Hessian. The strongest alignment corresponds to  $\langle(\mathbf{e}_1^P \cdot \mathbf{e}_2)^2\rangle \approx 0.4$ , which is only marginally larger than  $1/3$ . Moreover, all alignment results are virtually independent of  $R_\lambda$  as it was earlier the case for the alignment between vorticity and eigenvectors of pressure Hessian.

To rule out any anomalous behavior, Fig. 6 shows the PDFs of the alignment cosines. While the distributions are not exactly uniform, it can be seen that they are essentially consistent with the behavior anticipated from their second order moments in Table III, i.e., demonstrating some weak preferential alignment for moments larger than  $1/3$  (and vice versa). In all panels, the solid and dashed lines at  $R_\lambda = 1300$  and  $140$ , respectively, near perfectly coincide, showing that the alignment results are independent of  $R_\lambda$ .

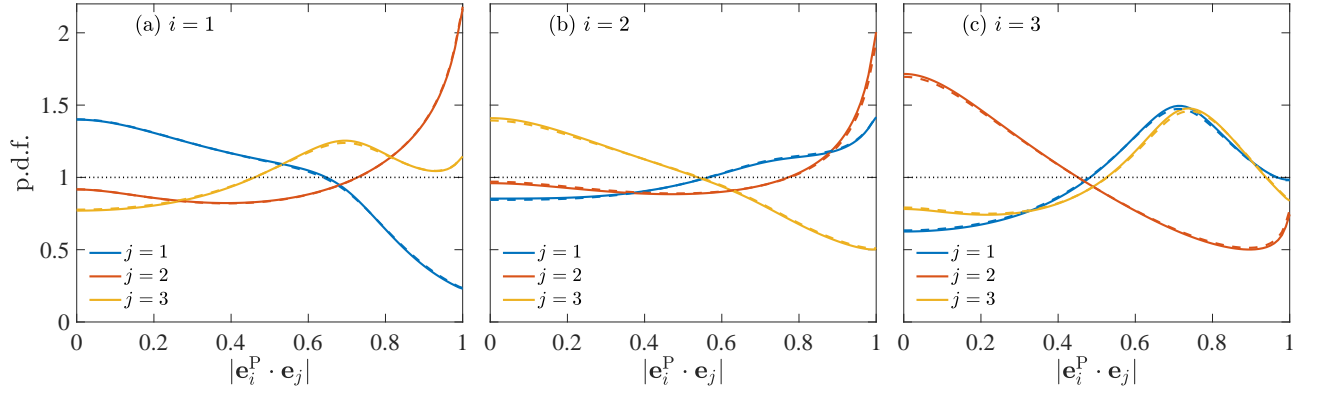


FIG. 6. Probability density function (p.d.f.) of alignment cosines between eigenvectors of pressure Hessian ( $\mathbf{e}_i^P$ ) and strain ( $\mathbf{e}_j$ ), at  $R_\lambda = 1300$  (solid lines) and  $R_\lambda = 140$  (dashed lines).

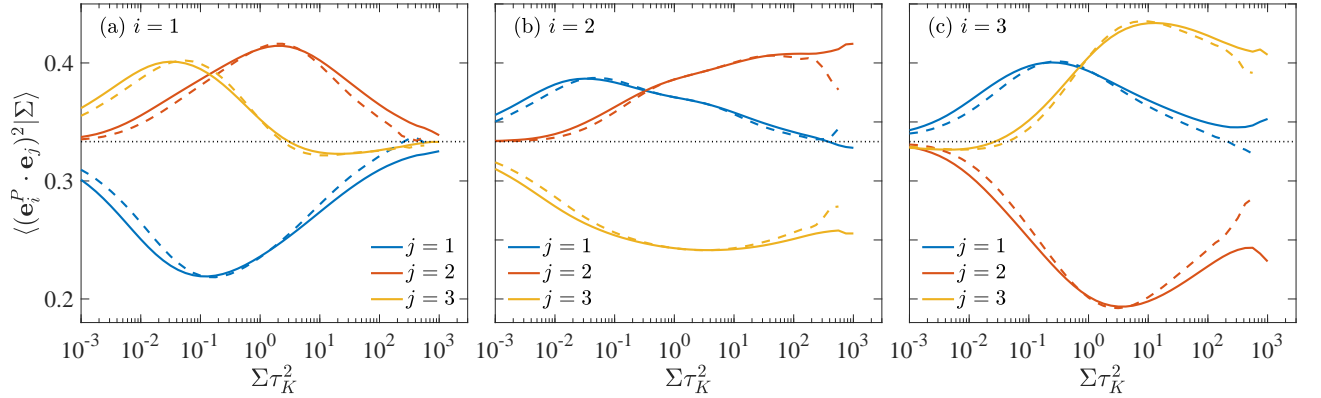


FIG. 7. Conditional expectation (given  $\Sigma$ ) of second moment of alignment cosines between eigenvectors of pressure Hessian ( $\mathbf{e}_i^P$ ) and strain ( $\mathbf{e}_j$ ), at  $R_\lambda = 1300$  (solid lines) and  $R_\lambda = 650$  (dashed lines).

## B. Conditional statistics

To analyze the extreme strain events, we now consider various statistics conditioned on  $\Sigma\tau_K^2$  (which equals  $\Sigma/\langle\Sigma\rangle$ ). Figure 7 shows the conditional alignment between eigenvectors of strain and pressure Hessian as measured by  $\langle(\mathbf{e}_i^P \cdot \mathbf{e}_j)^2|\Sigma\rangle$ . For clarity, we only show  $R_\lambda = 1300$  (solid lines) and  $R_\lambda = 650$  (dashed lines). The dependence on  $R_\lambda$  is very weak, and results at lower  $R_\lambda$  (not shown) essentially follow same trends. Overall, the alignment results indicate that there is no strong preferential alignment between strain and pressure Hessian, even when extreme events are considered. The strongest alignments, parallel and orthogonal, are respectively observed for  $j = 3$  and  $j = 2$ , both with  $i = 3$ , but the deviations from  $1/3$  remain weak.

The conditional expectations of the eigenvalues of the pressure Hessian, and of its deviatoric part, are shown in Figure 8a and b, respectively. In both cases, we observe that the first and third eigenvalues are strongly positive and negative respectively, and the second eigenvalue is very close to zero. The eigenvalues of pressure Hessian satisfy  $\langle(\lambda_1^P + \lambda_2^P + \lambda_3^P)|\Sigma\rangle = \langle(\Omega - \Sigma)|\Sigma\rangle$ . Since  $\langle\Omega|\Sigma\rangle \sim \Sigma$ , but with a prefactor which is slightly smaller than unity [20, 35], it follows that the sum of eigenvalues  $\lambda_i^P$  divided by  $\Sigma$  is a small, negative constant. Indeed, this is the observation in Fig. 8a, which shows that  $\langle-\lambda_3^P|\Sigma\rangle \gtrsim \langle\lambda_1^P|\Sigma\rangle$ , whereas  $\langle\lambda_2^P|\Sigma\rangle \approx 0$ . On the contrary, the sum of eigenvalues of the deviatoric part is exactly zero. Indeed, Fig. 8b conforms with this expectation, with  $\langle-\lambda_3^D|\Sigma\rangle \gtrsim \langle\lambda_1^D|\Sigma\rangle$  being still true, but  $\langle\lambda_2^D|\Sigma\rangle$  is weakly positive, ensuring that the sum of the eigenvalues is zero.

Figure 9 shows conditional expectation of the correlation  $S_{ij}H_{ij}$ , together with the individual contributions from the eigendirections of pressure Hessian; panel a shows the result for pressure Hessian and its eigenvalues and panel b shows the corresponding result for the deviatoric part. Note that despite  $S_{ij}H_{ij} = S_{ij}H_{ij}^D$ , the individual contributions from their respective eigendirections differ. Given the lack of any strong alignment between strain and pressure Hessian eigenvectors, it can be anticipated that the largest contribution to  $S_{ij}H_{ij}$  would arise from their largest eigenvalues, i.e., the product  $\lambda_3^P\lambda_3$  (or  $\lambda_3^D\lambda_3$ ). Additionally, this contribution would be positive, since both these eigenvalues are negative. Indeed, Fig. 9a-b confirms this expectation. For both panels, the largest contribution is positive and

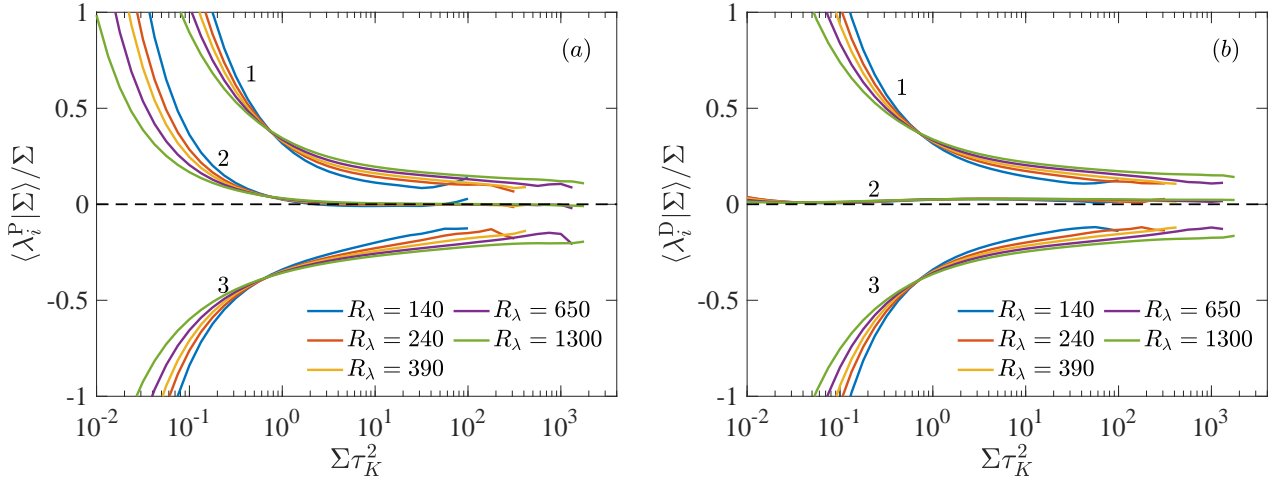


FIG. 8. (a) Conditional expectation (given  $\Sigma$ ) of the eigenvalues of pressure Hessian, at various  $R_\lambda$ . (b) Conditional expectation of the eigenvalues of the deviatoric part.

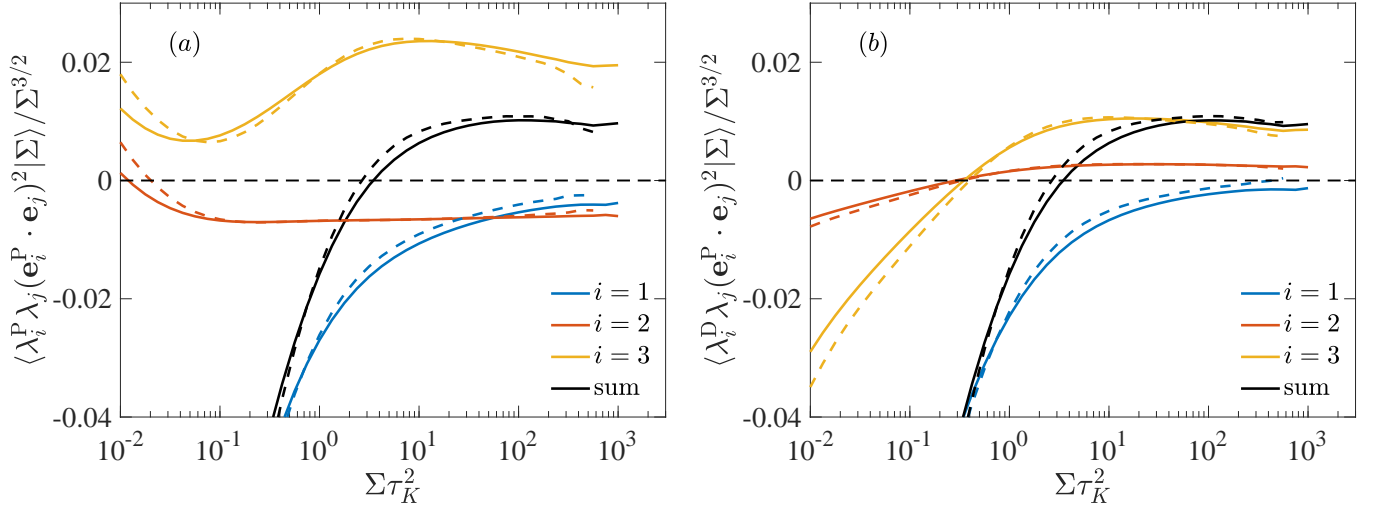


FIG. 9. Individual contributions to (a)  $\langle S_{ij} H_{ij} | \Sigma \rangle = \langle \lambda_i^P \lambda_j^P (\mathbf{e}_i^P \cdot \mathbf{e}_j^P)^2 | \Sigma \rangle$ , and (b)  $\langle S_{ij} H_{ij}^D | \Sigma \rangle = \langle \lambda_i^D \lambda_j^D (\mathbf{e}_i^D \cdot \mathbf{e}_j^D)^2 | \Sigma \rangle$ , from their eigendirections. Note, the summation is only implied over  $j$ , and results for each  $i$  are shown. The quantities have been rescaled by  $\Sigma^{3/2}$ . The solid lines are for  $R_\lambda = 1300$  and dashed lines for  $R_\lambda = 650$ . The black lines given the total sum over all eigendirections.

corresponds to  $i = 3$ . In contrast, the contribution for  $i = 1$  is negative, since it is dominated by the product  $\lambda_1^P \lambda_3$ , (or  $\lambda_1^D \lambda_3$  for panel b). The behavior for  $i = 2$  is not as straightforward to predict, since the alignments are nontrivial for this case. Interestingly, we observe that the contribution from  $i = 2$  is negative in panel a, but weakly positive in panel b. For large  $\Sigma$ , all the contributions (as divided by  $\Sigma^{3/2}$ ) appear approximately constant, implying a simple scaling [20].

The main observation from Fig. 9 is that the pressure Hessian term attenuates strong strain and amplifies weak strain (since the net effect has to be zero). Nevertheless, as evident from Eq. (7), strain amplification involves other nonlinear mechanisms. Their relative amplitudes were already compared in [20]. For completeness, Fig. 10 shows the conditional expectations of the various inviscid terms involved in the budget equation for strain (together with their corresponding signs). All terms are once again normalized by  $\Sigma^{3/2}$ . It can be seen that the self-amplification term is the largest contribution and the primary mechanism for generating intense strain. In contrast, the vortex stretching contribution always opposes strain amplification, whereas the pressure Hessian term opposes intense strain but amplifies weak strain. When considering strong strain events ( $\Sigma \tau_K^2 > 1$ ), the pressure Hessian term is noticeably weaker than vortex stretching term, and both are considerably weaker than the strain self-amplification term.

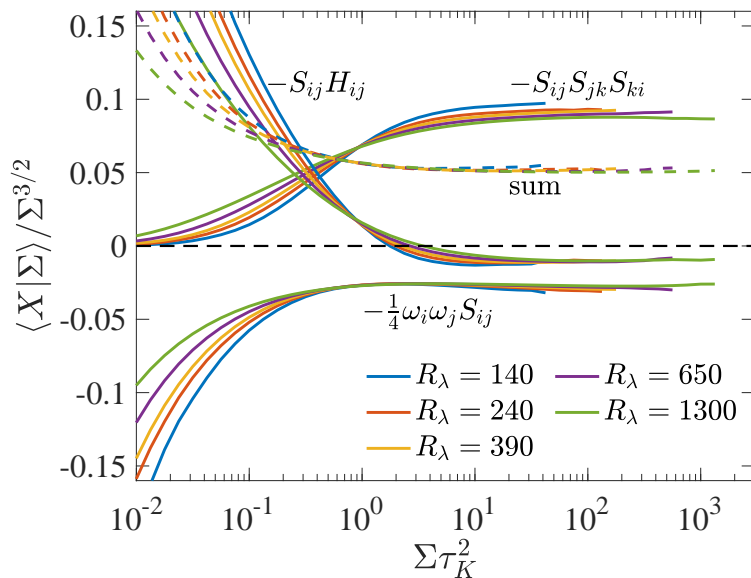


FIG. 10. Conditional expectations (given  $\Sigma$ ) of various inviscid terms on the r.h.s. of Eq. (7). All quantities are normalized by  $\Sigma^{3/2}$  revealing a plateau like behavior for  $\Sigma\tau_K^2 > 1$ .

## VI. SUMMARY AND CONCLUSIONS

The pressure field, via its Hessian tensor, plays a direct role in the dynamics of velocity gradient tensor  $A_{ij}$  in turbulence. Since pressure Hessian  $H_{ij}$  is a symmetric tensor, its effect on the amplification of strain  $S_{ij}$  (the symmetric part of  $A_{ij}$ ) is explicit. However, its influence on amplification of vorticity vector  $\omega_i$  (the skew-symmetric part of  $A_{ij}$ ) comes as a second order effect through the dynamics of the vortex stretching vector  $W_i = \omega_j S_{ij}$ . However, studies directly investigating the role of pressure Hessian on gradient amplification have been limited in the literature and when available, restricted to low Reynolds numbers. In this paper, utilizing a massive DNS database of isotropic turbulence across a wide range of Taylor-scale Reynolds numbers ( $140 \leq R_\lambda \leq 1300$ ), we systematically investigate various statistical correlations underpinning the role of pressure Hessian on gradient amplification and formation of extreme events.

Overall, pressure Hessian acts to deplete vortex stretching (and also strain amplification, which is discussed soon). Decomposing the pressure Hessian into its isotropic (local) and deviatoric (nonlocal) components reveals that the former opposes vortex stretching, whereas the latter favors it. There is strong cancellation between the two, such that the isotropic contribution ultimately dominates, although the net effect is significantly weaker than the nonlinear mechanism (which always enables vortex stretching). However, when the statistics are conditioned on enstrophy  $\Omega = \omega_i \omega_i$ , we find that the inhibiting effect of pressure Hessian becomes dominant over the nonlinear mechanism, essentially leading to net depletion of vortex stretching. This depletion, which comes from local isotropic part, suggests a natural connection to the self-attenuation mechanism recently identified in [21, 32] whereby it was shown that the self-induced local strain in regions of intense vorticity acts to attenuate further growth of vorticity. However, additional investigation is required to reinforce this connection, particularly by analyzing the dynamics of velocity gradients in the Lagrangian framework, which will be the subject of future work.

We further analyze the contribution of pressure Hessian to vortex stretching in its eigenframe. For the mean field, the sum of eigenvalues is zero, resulting in first (largest) and third (smallest) eigenvalues being nearly equal in magnitude, but opposite in sign; the second (intermediate) eigenvalue is weakly positive but essentially close to zero. No particular strong alignment is observed between vorticity and eigenvectors of pressure Hessian. However, when considering conditional statistics, the third eigenvalue becomes close to zero, and both first and second eigenvalues are positive. At the same time, vorticity near perfectly aligns with the third eigenvector (while being orthogonal to other two). Structurally, this conforms with the well known notion that intense vorticity in turbulence is arranged in tubes, which approximately correspond to Burgers vortex. However, key differences remain, which essentially give rise to the self-attenuation mechanism, as elucidated by [21]. Considering the deviatoric and isotropic components separately allows for a simpler interpretation of how pressure Hessian overall affects vortex stretching. Overall, not particularly strong dependence on Reynolds number is observed for all the statistics considered.

We also investigate the role of pressure Hessian on strain amplification, which is more direct, since both tensor are

symmetric. Overall, pressure Hessian does not contribute to the budget of strain, as their correlation is zero (using homogeneity). However, when considering conditional statistics, we find that pressure Hessian acts to oppose intense strain, but amplifies weak strain, essentially driving strain fluctuations towards the mean amplitude. Complementary to the analysis presented in [20], we focus here on the eigenframe of pressure Hessian. As before, the first and third eigenvalues of pressure Hessian are comparable in magnitude, but opposite in sign. This behavior also applies when conditioning on strain magnitude. No strong alignments are observed between eigenvectors of strain and pressure Hessian, both for unconditional and conditional fields. Because of this, the resulting behavior strain and pressure Hessian correlation can be deduced simply from the product of their eigenvalues. We contrast the strength of pressure Hessian term with other nonlinear mechanisms controlling strain amplification, viz. the self-amplification term and vortex stretching. Evidently, the self-amplification term always amplifies strain; however, vortex stretching always opposes it, with its magnitude significantly weaker. The opposition from pressure Hessian term is even weaker.

Finally, we note that many of the conditional statistics investigated here follow simple power law dependencies on vorticity or strain magnitude (when considering extreme events). We have identified these power laws in various figures as necessary. These results should prove valuable in statistical modeling of enstrophy or energy dissipation rate, particularly in PDF methods [50]. Additionally, the various conditional statistics of pressure Hessian should also provide valuable benchmarks for Lagrangian modeling of velocity gradient dynamics [6]. These aspects will be explored in future work.

### ACKNOWLEDGEMENTS

We gratefully acknowledge the Gauss Centre for Supercomputing e.V. for providing computing time on the supercomputers JUWELS and JUQUEEN at Jülich Supercomputing Centre (JSC), where the simulations and data analyses reported in this paper were performed.

- 
- [1] U. Frisch, *Turbulence: the legacy of Kolmogorov* (Cambridge University Press, Cambridge, 1995).
  - [2] K. S. Sreenivasan and R. A. Antonia, The phenomenology of small-scale turbulence, *Annu. Rev. Fluid Mech.* **29**, 435 (1997).
  - [3] G. Falkovich, K. Gawędzki, and M. Vergassola, Particles and fields in fluid turbulence, *Rev. Mod. Phys.* **73**, 913 (2001).
  - [4] J. M. Wallace, Twenty years of experimental and direct numerical simulation access to the velocity gradient tensor: What have we learned about turbulence?, *Phys. Fluids* **21**, 021301 (2009).
  - [5] A. Tsinober, *An Informal Conceptual Introduction to Turbulence* (Springer, Berlin, 2009).
  - [6] C. Meneveau, Lagrangian dynamics and models of the velocity gradient tensor in turbulent flows, *Annu. Rev. Fluid Mech.* **43**, 219 (2011).
  - [7] G. Falkovich, A. Fouxon, and M. G. Stepanov, Acceleration of rain initiation by cloud turbulence, *Nature* **419**, 151 (2002).
  - [8] P. E. Hamlington, A. Y. Poludnenko, and E. S. Oran, Intermittency in premixed turbulent reacting flows, *Phys. Fluids* **24**, 075111 (2012).
  - [9] D. Buaria, B. L. Sawford, and P. K. Yeung, Characteristics of backward and forward two-particle relative dispersion in turbulence at different Reynolds numbers, *Phys. Fluids* **27**, 105101 (2015).
  - [10] G. A. Voth and A. Soldati, Anisotropic particles in turbulence, *Annu. Rev. Fluid Mech.* **49**, 249 (2017).
  - [11] D. Buaria, M. P. Clay, K. R. Sreenivasan, and P. K. Yeung, Small-scale isotropy and ramp-cliff structures in scalar turbulence, *Phys. Rev. Lett.* **126**, 034504 (2021).
  - [12] A. N. Kolmogorov, The local structure of turbulence in an incompressible fluid for very large reynolds numbers, *Dokl. Akad. Nauk. SSSR* **30**, 299 (1941).
  - [13] J. D. Gibbon, M. Bustamante, and R. M. Kerr, The three-dimensional Euler equations: singular or non-singular?, *Nonlinearity* **21**, T123 (2008).
  - [14] C. R. Doering, The 3D Navier-Stokes problem, *Annu. Rev. Fluid Mech.* **41**, 109 (2009).
  - [15] C. Fefferman, Existence and smoothness of the Navier-Stokes equations (Clay Mathematical Institute, Cambridge, MA, 2006).
  - [16] K. K. Nomura and G. K. Post, The structure and dynamics of vorticity and rate of strain in incompressible homogeneous turbulence, *J. Fluid Mech.* **377**, 65 (1998).
  - [17] C. Kalelkar, Statistics of pressure fluctuations in decaying isotropic turbulence, *Phys. Rev. E* **73**, 046301 (2006).
  - [18] J. M. Lawson and J. R. Dawson, On velocity gradient dynamics and turbulent structure, *J. Fluid Mech.* **780**, 60–98 (2015).
  - [19] M. Carbone, M. Iovieno, and A. D. Bragg, Symmetry transformation and dimensionality reduction of the anisotropic pressure hessian, *J. Fluid Mech.* **900**, A38 (2020).
  - [20] D. Buaria, A. Pumir, and E. Bodenschatz, Generation of intense dissipation in high reynolds number turbulence, *Phil. Trans. R. Soc. A* **380**, 20210088 (2022).

- [21] D. Buaria, A. Pumir, and E. Bodenschatz, Self-attenuation of extreme events in Navier-Stokes turbulence, *Nat. Commun.* **11**, 5852 (2020).
- [22] W. T. Ashurst, A. R. Kerstein, R. M. Kerr, and C. H. Gibson, Alignment of vorticity and scalar gradient with strain rate in simulated Navier-Stokes turbulence, *Phys. Fluids* **30**, 2343 (1987).
- [23] D. Buaria, E. Bodenschatz, and A. Pumir, Vortex stretching and enstrophy production in high Reynolds number turbulence, *Phys. Rev. Fluids* **5**, 104602 (2020).
- [24] A. Tsinober, M. Ortenberg, and L. Shtilman, On depression of nonlinearity in turbulence, *Phys. Fluids* **11**, 2291 (1999).
- [25] J. Jiménez, A. A. Wray, P. G. Saffman, and R. S. Rogallo, The structure of intense vorticity in isotropic turbulence, *J. Fluid Mech.* **255** (1993).
- [26] F. Moisy and J. Jiménez, Geometry and clustering of intense structures in isotropic turbulence, *J. Fluid Mech.* **513**, 111 (2004).
- [27] S. S. Girimaji and S. B. Pope, A diffusion model for velocity gradients in turbulence, *Phys. Fluids A* **2**, 242 (1989).
- [28] P. L. Johnson and M. Wilczek, Multiscale velocity gradients in turbulence, *Annu. Rev. Fluid Mech.* , (to appear) (2023).
- [29] Y. Tian, D. Livescu, and M. Chertkov, Physics-informed machine learning of the Lagrangian dynamics of velocity gradient tensor, *Phys. Rev. Fluids* **6**, 094607 (2021).
- [30] D. Buaria and K. R. Sreenivasan, Forecasting small scale dynamics of fluid turbulence using deep neural networks, *Proc. Nat. Acad. Sci.* **120**, e2305765120 (2023).
- [31] P. E. Hamlington, J. Schumacher, and W. J. A. Dahm, Direct assessment of vorticity alignment with local and nonlocal strain rates in turbulent flows, *Phys. Fluids* **20**, 111703 (2008).
- [32] D. Buaria and A. Pumir, Nonlocal amplification of intense vorticity in turbulent flows, *Phys. Rev. Research* **3**, L042020 (2021).
- [33] D. G. Vlaykov and M. Wilczek, On the small-scale structure of turbulence and its impact on the pressure field, *J. Fluid Mech.* **861**, 422–446 (2019).
- [34] D. Buaria, A. Pumir, E. Bodenschatz, and P. K. Yeung, Extreme velocity gradients in turbulent flows, *New J. Phys.* **21**, 043004 (2019).
- [35] D. Buaria and A. Pumir, Vorticity-strain rate dynamics and the smallest scales of turbulence, *Phys. Rev. Lett.* **128**, 094501 (2022).
- [36] K. Ohkitani and S. Kishiba, Nonlocal nature of vortex stretching in an inviscid fluid, *Phys. Fluids* **7**, 411 (1995).
- [37] D. Buaria and K. R. Sreenivasan, Dissipation range of the energy spectrum in high Reynolds number turbulence, *Phys. Rev. Fluids* **5**, 092601(R) (2020).
- [38] D. Buaria and K. R. Sreenivasan, Intermittency of turbulent velocity and scalar fields using three-dimensional local averaging, *Phys. Rev. Fluids* **7**, L072601 (2022).
- [39] D. Buaria and K. R. Sreenivasan, Lagrangian acceleration and its Eulerian decompositions in fully developed turbulence, *Phys. Rev. Fluids* **8**, L032601 (2023).
- [40] R. S. Rogallo, Numerical experiments in homogeneous turbulence, NASA Technical Memo **81315** (1981).
- [41] G. K. Batchelor, *The theory of homogeneous turbulence* (Cambridge university press, 1953).
- [42] R. Betchov, An inequality concerning the production of vorticity in isotropic turbulence, *J. Fluid Mech.* **1**, 497 (1956).
- [43] R. M. Kerr, Higher-order derivative correlations and the alignment of small-scale structures in isotropic numerical turbulence, *J. Fluid Mech.* **153**, 31 (1985).
- [44] A. Gylfason, S. Ayyalasomayajula, and Z. Warhaft, Intermittency, pressure and acceleration statistics from hot-wire measurements in wind-tunnel turbulence, *J. Fluid Mech.* **501**, 213 (2004).
- [45] D. Buaria and K. R. Sreenivasan, Scaling of acceleration statistics in high Reynolds number turbulence, *Phys. Rev. Lett.* **128**, 234502 (2022).
- [46] T. Ishihara, Y. Kaneda, M. Yokokawa, K. Itakura, and A. Uno, Small-scale statistics in high resolution of numerically isotropic turbulence, *J. Fluid Mech.* **592**, 335 (2007).
- [47] J. M. Burgers, A mathematical model illustrating the theory of turbulence, *Adv. Appl. Mech.* **1**, 171 (1948).
- [48] B. Andreotti, Studying Burgers' models to investigate the physical meaning of the alignments statistically observed in turbulence, *Phys. Fluids* **9**, 735 (1997).
- [49] Y. Choi, B. G. Kim, and C. Lee, Alignment of velocity and vorticity and the intermittent distribution of helicity in isotropic turbulence, *Phys. Rev. E* **80**, 017301 (2009).
- [50] S. B. Pope, *Turbulent Flows* (Cambridge University Press, 2000).